

Contents lists available at ScienceDirect

# Petroleum Science

journal homepage: www.keaipublishing.com/en/journals/petroleum-science



# Original Paper

# A dual-model dual-grid upscaling method for solid-based thermalreactive-compositional flow simulations in fractured oil shale reservoirs



Qi-Zhi Tan <sup>a, b</sup>, Shu-Yang Liu <sup>a, b, \*</sup>, Yan-Ji Wang <sup>b, c, d</sup>, Hang-Yu Li <sup>a, b</sup>, Jun-Rong Liu <sup>a, b</sup>, Wen-Yue Sun <sup>a, b</sup>

- <sup>a</sup> Key Laboratory of Unconventional Oil & Gas Development (China University of Petroleum (East China)), Ministry of Education, Qingdao, 266580, Shandong, China
- <sup>b</sup> School of Petroleum Engineering, China University of Petroleum (East China), Qingdao, 266580, Shandong, China
- <sup>c</sup> College of Artificial Intelligence, China University of Petroleum (Beijing), Beijing, 102249, China
- <sup>d</sup> Hainan Institute of China University of Petroleum (Beijing), Sanya, 572024, Hainan, China

### ARTICLE INFO

#### Article history: Received 6 August 2024 Received in revised form 21 March 2025 Accepted 21 March 2025 Available online 22 March 2025

Edited by Yan-Hua Sun

Keywords:
Upscaling
Thermal-reactive-compositional flow
EDFM
Oil shale
In-situ conversion process

#### ABSTRACT

Simulation of thermal-reactive-compositional flow processes is fundamental to the thermal recovery of ultra-heavy hydrocarbon resources, and a typical oilfield practice is the in-situ conversion process (ICP) implemented in oil shale exploitation. However, accurately capturing the intricate flow dynamics of ICP requires a large number of fine-scale grid-blocks, which renders ICP simulations computationally expensive. Apart from that, plenty of oil shale reservoirs contain natural fractures or require hydraulic fracturing to enhance fluid mobility, creating further challenges in modeling pyrolysis reactions in both rock matrices and fractures. Targeted at the above issues, this work proposes a novel dual-model dualgrid upscaling (DDU) method specifically designed for solid-based thermal-reactive-compositional flow simulations in fractured porous media. Unlike existing upscaling techniques, the DDU method incorporates the upscaling of fracture grids using the embedded discrete fracture modeling (EDFM) approach and introduces a new concept of simplified models to approximate fine-scale results, which are used to correct reaction rates in coarse-scale grids. This method uniquely achieves efficient upscaling for both matrix and fracture grids, supports both open-source and commercial simulation platforms without modifying source codes, and is validated through 3D ICP models with natural fractures. The results indicate that the application of the DDU method can provide a close match with the fine-scale simulation results. Moreover, the DDU method has drastically improved the computational efficiency and speeded up the fine-scale simulation by 396-963 times. Therefore, the proposed DDU method has achieved marked computational savings while maintaining high simulation accuracy, which is significant for the development efficiency and production forecasting of oil shale reservoirs.

© 2025 The Authors. Publishing services by Elsevier B.V. on behalf of KeAi Communications Co. Ltd. This is an open access article under the CC BY license (http://creativecommons.org/licenses/by/4.0/).

# 1. Introduction

Shale oil is an abundant unconventional hydrocarbon resource widely distributed around the globe with an estimated technically recoverable amount of  $1.4 \times 10^{12}$  tons, which is 3 times larger than the amount of conventional oil reserves (Zhao et al., 2018). However, a significant portion of shale oil is of low to medium maturity and is retained in a combustible solid material called kerogen,

which is the main organic component in oil shale formation (Zhao et al., 2020). Kerogen can be pyrolyzed into mobile hydrocarbons at approximately 343–371 °C (Fowler and Vinegar, 2009; Hazra et al., 2013). Based on this principle, a typical method for the exploitation of low to medium shale oil is known as in-situ conversion process (ICP) that heats the oil shale formation to the pyrolysis temperature of kerogen. Shell Oil Co. (Shell) first put this approach into practice by using vertical electric heaters in Green River oil shale (Fowler and Vinegar, 2009; Shen, 2009). Following that, ExxonMobil also implemented this method by hydraulically fracturing the oil shale formation and filling the fractures with electrically conductive

E-mail address: shuyang\_liu@126.com (S.-Y. Liu).

<sup>\*</sup> Corresponding author.

proppants (Liu et al., 2023). Detailed application of ICP techniques in oil shale development can be found in Fowler and Vinegar (2009), Kang et al. (2020) and Liu et al. (2023). In China, for instance, the amount of shale oil that can be recovered by ICP is estimated to be 70 to 90 billion tons (Yang et al., 2019), highlighting the significant role of oil shale ICP in the energy supply.

Several endeavors have been made to replicate the production results of Shell's and ExxonMobil's ICP using reservoir modeling software, such as Stanford's General Purpose Research Simulator (GPRS) (Fan et al., 2010), Texas A&M Flow and Transport Simulator (FTSim) (Lee et al., 2016) and CMG-STARS (Hazra et al., 2013; Perez—Perez et al., 2019; Shen, 2009). However, accurately simulating the intricate thermal-reactive-compositional flow processes in ICP necessitates fine-scale grids, which is computationally expensive. Additionally, it is reported that natural fractures exist in oil shale formation, which further increase the computational cost of ICP simulation (Fowler and Vinegar, 2009). Considering that, reliable upscaling techniques are required to model ICP by coarse-scale grids while preserving reasonable simulation accuracy.

A great number of upscaling techniques developed so far typically focus on isothermal-nonreactive flow problems (Barker and Thibeau, 1997; Durlofsky, 2005; Farmer, 2002; Zhang et al., 2021). while that address thermal-reactive-compositional flow simulations are relatively scarce. A recent effort for the upscaling of ICP simulations was presented in Aouizerate et al. (2012). This work proposed a local well model (LWM) that uses coarse-scale boundary conditions and fine-scale solutions to derive the coarse-scale heater-well indices. The upscaling of heater-well indices was also considered in Li et al. (2016). This work introduced a multiscale upscaling method that refines coarse-scale properties to fine-scale grids at every simulation timestep, and then compute the fine-scale reaction rates and heater temperature to calibrate the coarse-scale reaction parameters and heater-well indices. Similarly, Alpak and Vink (2016) developed a local-global multiscale upscaling procedure for coarse-scale thermal and flow properties, including thermal transmissibility, heater-well indices and permeability. This method was applied on 2D ICP models and achieved speeded up the finescale simulation by 5.5 times. However, the above techniques were mostly employed on 2D ICP models, and were rarely applied on 3D simulations. Moreover, these methods all require modifications on the internal source code of simulators, which are inaccessible to the users of closed-source commercial modeling software. This significantly limits their widespread industrial application.

Likewise, the existing upscaling techniques aimed at fracture modeling pivot only on isothermal-nonreactive simulations. Chen et al. (2015) categorized these techniques into analytical upscaling and flow-based upscaling. The former was proposed by Oda (1985) who calculated the equivalent permeability tensors of fractures based on their geometric characteristics, such as aperture. orientation, and length. This method requires less computational cost compared to flow-based upscaling, but tends to overestimate the equivalent permeability and yield less accurate simulation results (Ahmed and Geiger, 2012). To address this overestimation, Lee et al. (2001) developed a hierarchical approach that classifies fractures into short, medium, and long length scales. This method accounted for the permeability contribution of short fractures through analytical formula, applied a boundary element method for medium fractures, and explicitly represented long fractures as fluid conduits. This approach not only improves the representation of directional, enhanced permeability but also captures efficient fluid transport facilitated by long fractures. As for flow-based

upscaling, Long et al. (1982) first applied linear pressure boundary conditions to measure the equivalent permeability tensor of fractured porous media in structured grids. Later, Chen et al. (2015) extended this method to unstructured triangular using multi-point flux approximation (MPFA). This approach considered fluid flow across multiple boundaries, and the total flow rate in each coordinate direction is the sum of flow rates in that direction through these boundaries. Similar attempt on the upscaling of fracture porous media in unstructured grids can also be found in Koudina et al. (1998), who solved 2D pressure equations for fracture flows to derive the equivalent permeability of 3D triangular mesh. However, the above methods assume that the matrix is impermeable, and thus mass exchange only occurs between matrices and fractures or within fractures. Targeted at this issue, Bogdanov et al. (2003) considered the matrix permeability based on the upscaling method of Koudina et al. (1998). Following that, Gong et al. (2006) and Karimi-Fard et al. (2006) employed two-point flux approximation (TPFA) method in transmissibility upscaling to represent the fracture in 2D and 3D dual-continuum models with the consideration for gravity and capillary pressure. Similarly, Sherratt et al. (2020) developed a fracture upscaling model (FUM) for dualcontinuum simulators. This work determined upscaled fracture permeability through the averaged geological properties weighted by fracture area. The upscaled fracture network could then be exported to dual-continuum simulators based on finite difference method to calculate the mass exchange between matrices and fractures.

In a nutshell, the previous upscaling techniques regarding thermal-reactive-compositional flow simulations have largely overlooked the upscaling of fracture grids and rarely addressed 3D models. To bridge these gaps, this paper presents a novel dualmodel dual-grid upscaling (DDU) method for solid-based thermal-reactive-compositional flow simulations in fractured porous media. The DDU method is the first to integrate the upscaling of both matrix and fracture grids with compatibility to the EDFM approach, a widely adopted non-intrusive fracture modeling technique (Moinfar et al., 2012, 2013; Xu et al., 2017, 2019, 2020; Yu et al. 2021). Furthermore, this method is distinctive in its ability to operate with existing modeling software by integrating thermalreactive-compositional flow simulators with externally executed Python programs, eliminating the need for source code modifications. These features make the DDU method applicable to a wide range of simulation scenarios. The layout of this paper is as follows: first, we describe the governing equations and the upscaling framework for ICP simulations involving natural fractures; second, the performance and reliability of the proposed DDU method are analyzed through multiple 3D simulation cases; finally, the conclusions of this paper is presented.

#### 2. Governing equations

Prior to the elaboration of the DDU method, this section presents the key governing equations for the coupled thermal-reactive-compositional flow processes in ICP simulations.

### 2.1. Mass- and energy-conservation equations

The mass-conservation equation for fluid component c in thermal-reactive-compositional flow modeling is expressed as follows (Li et al., 2016):

$$\frac{\partial}{\partial t} \left[ V_f \sum_{j} (\rho_j S_j M_{cj}) \right] = \sum_{l=1}^{n_f} \left[ \sum_{j} (\lambda_j \rho_j M_{cj} \Delta \Phi_j) \right] + \phi \sum_{l=1}^{n_f} (\rho_j \Delta M_{cj}) + V \sum_{k=1}^{n_f} r(s'_{kc} - s_{kc}) + \sum_{j} (\rho_j q_j M_{cj}),$$
(1)

where  $\partial t$  stands for the unit simulation timestep, s:  $V_f$  is the pore volume of fluid phase, m<sup>3</sup>; V is the single grid-block volume, m<sup>3</sup>;  $\rho_i$ (i = w for water, o for oil, g for gas or s for solid) represents the mass density of phase j, kg/m<sup>3</sup>;  $S_i$  is the saturation of phase j, fraction;  $M_{ci}$ is the mole fraction of component c in phase j, fraction;  $\Delta M_{ci}$  is the difference in the mass fraction of component *c* in phase *j* between the adjacent region and the current region of interest, fraction;  $n_{\rm f}$ denotes the number of neighboring regions or grid-block faces;  $n_r$  is the total number of chemical reactions;  $\Delta \Phi_i$  denotes the potential difference of phase i between the node of the adjacent region and the node of the current region of interest, kPa;  $\phi$  is the porosity of fluid phase, fraction;  $s'_{kc}$  and  $s_{kc}$  are the stoichiometric coefficients for component c as product and reactant in kth (k = 1, 2, 3, ...)chemical reaction, dimensionless; r is the volumetric rate of chemical reaction k, which is calculated by the Arrhenius kinetic model,  $kg/(m^3 \cdot s)$ ;  $q_i$  is the sink and source term of phase j,  $m^3/s$ ; and  $\lambda_i$  is the transmissibility of phase j between two neighboring grid-blocks, which is provided by

$$\lambda_j = K(\phi) \left( \frac{k_{rj}}{\mu_j} \right), \tag{2}$$

where  $K(\phi)$  denotes current absolute rock permeability, m<sup>2</sup>;  $k_{ri}$  is the relative permeability of phase j, dimensionless; and  $\mu_j$  is the dynamic viscosity of phase j, mPa·s.

The well-production rate for fluid phase i is given by

$$q_j = I_j \Big( P_{\text{wf}} - P \Big), \tag{3}$$

where  $I_i$  is the well index of fluid phase j,  $m^3/(kPa \cdot s)$ ;  $P_{wf}$  is the wellbore pressure, kPa; and P is the node pressure of the current grid-block of interest, kPa.

The mass-conservation equation for immobile solid component c is given by (Li et al., 2016)

$$\frac{\partial C_c}{\partial t} = \sum_{k=1}^{n_f} (s'_{kc} - s_{kc}) r_k, \tag{4}$$

where  $C_c$  is the mass concentration of solid component c, kg/m<sup>3</sup>. The energy-conservation equation is expressed as (Li et al., 2016)

$$\begin{split} \frac{\partial}{\partial t} \left[ V_{f} \sum_{j} (\rho_{j} S_{j} U_{j}) + V_{v} C_{s} U_{s} + V_{r} U_{r} \right] &= \sum_{l=1}^{n_{f}} (\lambda_{j} \rho_{j} H_{j} \Delta \Phi_{j}) + \sum_{l=1}^{n_{f}} (\kappa \Delta T) \\ &+ \sum_{k=1}^{n_{r}} (H_{rk} r_{k}) + \sum_{i} (\rho_{j} q_{j} H_{j}) - q^{H}, \end{split}$$

where  $V_{v}$  is the total pore volume of both fluid and reactive solid components,  $m^3$ ;  $V_r$  is the volume of inert rock matrix,  $m^3$ ;  $U_i$ represents the mass internal energy of phase j, J/kg;  $U_s$  is the mass internal energy of reactive solid components, J/kg;  $U_r$  is the volumetric internal energy of non-reactive rock matrix,  $J/m^3$ ;  $C_s$  is the

total mass concentration of solid components,  $kg/m^3$ ;  $H_i$  is the mass enthalpy of phase j, J/kg;  $\kappa$  is comprehensive thermal conductivity of saturated rock matrix,  $J/(m \cdot s \cdot K)$ ;  $\Delta T$  is the temperature difference between the current grid-block of interest and its neighboring block, °C or K;  $H_{rk}$  is the mass enthalpy of reaction k, J/kg; and  $q^H$  is the energy input from heater wells, I/s.

### 2.2. Kinetic model

In this paper, kerogen is set as the primary solid component that pyrolyzes into lighter fluid components under high temperature. and the reaction rates are calculated by the Arrhenius kinetic model (Arrhenius, 1889; Laidler, 1984; Lee et al., 2016; Nagy and Turanyi, 2011; Wellington et al., 2005). The reaction rate of the kerogen pyrolysis reaction at temperature T is given by

$$r = \gamma \exp\left(\frac{-E}{RT}\right) (\phi_{\mathbf{v}}C)^n,\tag{6}$$

where  $\gamma$  is the reaction frequency factor, 1/s; E is the activation energy, J/mol; T is the absolute temperature, K; R is the gas constant, 8.314 J/(mol·K);  $\phi_V$  is the void porosity (the total porosity of fluid and reactive solid components), fraction; C is the mass concentration of kerogen,  $kg/m^3$ ; n is the reaction order, which is set as 1 in this study.

# 2.3. Calculation of reservoir properties

Permeability as a function of porosity. In this study, the absolute rock permeability (K) is a function of fluid porosity via the Carman-Kozeny formula (Carman, 1997), which is given by

$$K = K_0 \left(\frac{\phi}{\phi_0}\right)^{CKpower} \left(\frac{1-\phi_0}{1-\phi}\right)^2,\tag{7}$$

where  $K_0$  denote the initial absolute permeability of rock,  $m^2$ ;  $\phi$  and  $\phi_0$  is the current and initial fluid porosity, separately, fraction; CKpower is the Carman-Kozeny exponent, which is set to be 5 in this work. As the fluid porosity reduces, the absolute rock permeability decreases exponentially.

Thermal conductivity as a function of porosity and phase saturation. The comprehensive thermal conductivity of saturated rock matrix is expressed as (Bejan, 2013)

$$\kappa = \phi \sum_{i} (S_{j} \kappa_{j}) + (\phi_{v} - \phi) \kappa_{s} + (1 - \phi_{v}) \kappa_{r}, \tag{8}$$

where  $\kappa_i$  stands for the thermal conductivity of phase j,  $J/(m \cdot s \cdot K)$ ; and  $\kappa_r$  is the thermal conductivity of inert rock matrix,  $J/(m \cdot s \cdot K)$ .

# 2.4. Embedded discrete fracture modeling

The embedded discrete fracture modeling (EDFM) is an efficient and non-intrusive method for fracture modeling developed by Lee et al. (2001), Li and Lee (2008), and Moinfar et al. (2012, 2013). The EDFM method discretizes each fracture segments into an independent grid from the surrounding rock matrix and other fracture segments. This approach facilitates the modification of fracture grid properties during simulation, which is fundamental to the implementation of the proposed DDU method. Therefore, this paper utilizes the EDFM to simulate reservoir fractures. The EDFM method calculates the transmissibility between matrix and fracture blocks by (Moinfar et al., 2012, 2013)

$$T_{m-f} = \frac{A_{m-f} \cdot k_{m-f}}{d_{m-f}},\tag{9}$$

where  $A_{\rm m-f}$  is the surface area of the fracture segment contained in the matrix block, m<sup>2</sup>;  $k_{\rm m-f}$  is the harmonic average of matrix permeability and fracture permeability, m<sup>2</sup>; and  $d_{\rm m-f}$  is the average normal distance between the matrix and fracture blocks, as given by

$$d_{\mathbf{m-f}} = \frac{\int_{V} x_{\mathbf{n}} dV}{V},\tag{10}$$

where dV represents the finite volume element of a grid-block,  $m^3$ ; and  $x_n$  is the normal distance of the finite volume element from the fracture plane, m. In terms of the connection between two fracture grids, their transmissibility is also computed through a harmonic average formula:

$$T_{f-f} = \frac{T_{f1} \cdot T_{f2}}{T_{f1} + T_{f2}},\tag{11}$$

$$T_{\rm f1} = \frac{k_{\rm f1}a_{\rm f1}l}{d_{\rm f1}}, \quad T_{\rm f2} = \frac{k_{\rm f2}a_{\rm f2}l}{d_{\rm f2}},$$
 (12)

where  $k_{\rm f}$  is the fracture permeability, m<sup>2</sup>;  $a_{\rm f}$  is the fracture aperture, m; l stands for the length of the intersection line that is perpendicular to the normal vectors of the two intersecting fracture planes, m.

# 3. Upscaling methodology

This work develops a dual-model dual-grid upscaling (DDU) method to realize accurate coarse-scale simulations for solid-based thermal-reactive-compositional flow problems. The main idea of this method is illustrated in Fig. 1. This method proposed simplified models to approximate the temperature evolution of the models involving the coupled thermal-reactive-compositional flow processes (hereinafter referred to as "full-physics models"). Meanwhile, coarse-scale full-physics simulations are leveraged to improve the accuracy of the temperature evolution in simplified models through a temperature compensation process. Following that, the simulation results of grid temperature in fine-scale simplified models are utilized to derive the reaction rates of fine-scale full-physics grids, which will subsequently be employed to correct the reaction rates of coarse-scale full-physics grids.

The detailed workflow of the DDU method for thermal-reactive-compositional flow simulations is expounded as follows:

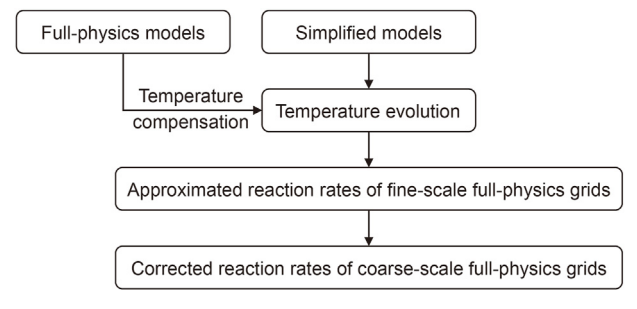


Fig. 1. The main idea of the DDU method.

Step 1. Establishment of the mapping between coarse-scale and fine-scale grids. For each coarse-scale matrix (or fracture) grid, identify all fine-scale matrix (or fracture) grids that correspond spatially, thereby establishing a mapping between coarse-scale and fine-scale grids. It is important to note that the matrix and fracture grids are mapped separately, as fractures are modeled as independent grid blocks, similar to matrix blocks, in the EDFM method. For instance, as shown in Fig. 2, the coarse-scale matrix blocks in both Situations 1 and 2 contain 36 fine-scale matrix blocks; however, the coarse-scale fracture block in Situation 1 corresponds spatially to 22 fine-scale fracture blocks, while that in Situation 2 corresponds to only 1 fine-scale fracture block.

**Step 2. Constructions of simplified models.** Build simplified coarse-scale and fine-scale models by setting the porosity of coarse-scale and fine-scale models to zero. Since the porosity is zero, the simplified models only include the heat conduction process and do not contain the fluid flow process, resulting in significantly faster simulation speeds compared to the full-physics models. This approximation is valid attributed to the low fluid porosity and permeability of oil shale, and thus the heat conduction process is less influenced by the multiphase flow in the full-physics models.

**Step 3. Temperature compensation.** Due to the omission of the heat transfer of fluid phase in the simplified models, discrepancies exist in the grid temperatures between the simplified models and the full-physics models. To address this issue, a temperature compensation procedure is performed according to Steps 3.1 through 3.3.

Step 3.1 Firstly, simulate the full-physics coarse-scale model, and the simplified coarse-scale and fine-scale models to obtain the temperature evolution of these models.

The relationship between the grid-block temperature in the full-physics models and that in the simplified models is defined as

$$T_{\text{coarse}i}^{\text{ful}} = T_{\text{coarse}i}^{\text{sim}} + \Delta T_{\text{coarse}i}^{t},$$
 (13)

$$T_{\text{fine}i}^{\text{ful}} = T_{\text{fine}i}^{\text{sim}t} + \Delta T_{\text{fine}i}^{t}, \tag{14}$$

where  ${}^t_i T^{\text{ful}}_{\text{coarse}}$  and  ${}^t_i T^{\text{sim}}_{\text{coarse}}$  represent the temperature of block i ( $i=1,2,3,\ldots$ ) in the full-physics and simplified coarse-scale models at timestep t ( $t=1,2,3,\ldots$ ), respectively;  $\Delta^t_i T_{\text{coarse}}$  is the temperature difference between  ${}^t_i T^{\text{ful}}_{\text{coarse}}$  and  ${}^t_i T^{\text{sim}}_{\text{coarse}}$ . Similarly,  ${}^t_i T^{\text{ful}}_{\text{fine}}$  and  ${}^t_i T^{\text{sim}}_{\text{fine}}$  stand for the temperature of block i in the full-physics and simplified fine-scale models at timestep t, individually; and  $\Delta^t_i T^{\text{sim}}_{\text{fine}}$  is the temperature difference between  ${}^t_i T^{\text{ful}}_{\text{fine}}$  and  ${}^t_i T^{\text{sim}}_{\text{fine}}$ .

Step 3.2 Secondly, calculate coarse-scale  $\Delta_i^t T_{\text{coarse}}$  based on  ${}^t_i T_{\text{ful}}^{\text{ful}}$  and  ${}^t_i T_{\text{coarse}}^{\text{imple}}$  that are derived from Step 3.1. Step 3.3 Lastly, for each coarse-scale block i and its corresponding fine-scale blocks, use  $\Delta_i^t T_{\text{coarse}}$  as the approximate values of  $\Delta_i^t T_{\text{fine}}$ , and add them on  ${}^t_i T_{\text{fine}}^{\text{sim}}$  of the corresponding fine-scale blocks to obtain the approximate values of  ${}^t_i T_{\text{fine}}^{\text{ful}}$  for these fine-scale blocks.

**Step 4. Computation of reaction rates and kerogen concentration.** Using the approximate values of  ${}_{i}^{t}T_{\mathrm{fine}}^{\mathrm{ful}}$  derived from Step 3, iteratively calculate the reaction rates and kerogen concentration of all fine-scale blocks (Li et al., 2015). The iteration process is expounded from Steps 4.1 through 4.4.

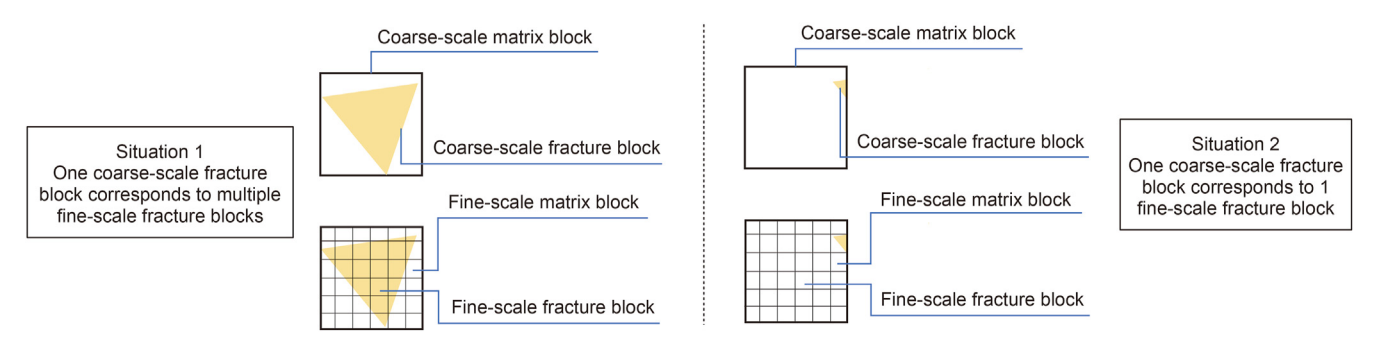


Fig. 2. The mapping relationship between coarse-scale fracture blocks and fine-scale fracture blocks.

Step 4.1 At the first timestep, initialize the values of reaction frequency factor, activation energy, void porosity, and kerogen concentration for all fine-scale grid-blocks. Step 4.2 For timestep t+1, the reaction rate of fine-scale

Step 4.2 For timestep t+1, the reaction rate of fine-scale block i is given by

$$r_{\text{fine}}_{i}^{t+1} = \gamma_{\text{fine}} \exp\left(-\frac{E}{R \cdot T_{\text{fine}}^{\text{ful}}}\right) \left(\phi_{\text{V}} \cdot C_{\text{fine}}_{i}^{t}\right),$$
 (15)

where  $_i^{t+1}r_{\rm fine}$  is the reaction rates of fine-scale block i at timestep t+1;  $\gamma_{\rm fine}$  is the fine-scale reaction frequency factor, which stays the same as the initial value of the given chemical reaction;  $_i^tC_{\rm fine}$  stands for the fine-scale kerogen concentration at timestep t.

Step 4.3 Update the fine-scale kerogen concentration at timestep t+1 by

$$C_{\text{fine}_{i}}^{t+1} = C_{\text{fine}_{i}}^{t} - r_{\text{fine}_{i}}^{t+1} \cdot \Delta t_{t}, \tag{16}$$

where  $\Delta^t t$  indicates the time duration of timestep t.

Step 4.4 Progress from timestep t to t+1, and repeat Steps 4.2 and 4.3 to the last timestep.

**Step 5.** Calculation of the average reaction rates of fine-scale **grids.** Based on the calculated reaction rates for all fine-scale grids, for each coarse-scale grid, compute the average reaction rates of all the fine-scale grids within this coarse-scale grid (hereinafter referred to as "the average fine-scale reaction rates", and is denoted by " ${}^t\bar{l}_{\text{fine}}$ ").

**Step 6. Upscaling simulation.** Re-simulate the full-physics coarse-scale model; at each simulation timestep, adjust the reaction frequency factor  $\gamma$  for each coarse-scale block to match the corresponding average fine-scale reaction rates. The adjustment of  $\gamma$  is implemented in Steps 6.1 through 6.3.

Step 6.1 Initialize the values of reaction frequency factor, activation energy, void porosity, and kerogen concentration for coarse-scale blocks at the first timestep.

Step 6.2 For timestep t+1, the reaction rate of coarse-scale block i is expressed as

$$_{i}^{t+1}r_{\text{coarse}} = _{i}^{t} \gamma_{\text{coarse}}^{*} \exp\left(-\frac{E}{R \cdot _{i}^{t} T_{\text{coarse}}^{\text{tul}}}\right) \left(\phi_{v} \cdot _{i}^{t} C_{\text{coarse}}\right),$$
(17)

where  $_{i}^{t+1}r_{\text{coarse}}$  is the reaction rate of coarse-scale block i at timestep t+1;  $_{i}^{t}\gamma_{\text{coarse}}^{*}$  is the adjusted reaction frequency factor of coarse-scale block i at timestep t;  $_{i}^{t}C_{\text{coarse}}$  represents the coarse-scale kerogen concentration at timestep t, which is obtained from

the results of coarse-scale simulation at timestep t.

Step 6.3 Following that, calculate the adjustment factor of  $\gamma$  for each coarse-scale block through

$$_{i}^{t+1}\alpha = \frac{_{i}^{t+1}r_{\text{fine}}}{_{t+1}^{t+1}r_{\text{coarse}}},$$
(18)

where  $_{i}^{t+1}\alpha$  stands for the adjustment factor of coarse-scale block i at timestep t+1.

Step 6.4 Consequently, the adjusted reaction rate for coarsescale block i is given by

$$_{i}^{t+1}\gamma_{\text{coarse}}^{*} = _{i}^{t+1}\alpha_{i}^{*}\gamma_{\text{coarse}}^{*}, \tag{19}$$

where  $i^{t+1}\gamma_{\text{coarse}}^*$  denotes the adjusted reaction frequency factor of coarse-scale block i for timestep t+1.

Step 6.5 Finally, substitute  $i^{t+1}\gamma_{\text{coarse}}^*$  for the original coarsescale reaction rates and simulate the coarse-scale model at timestep t+1. Repeat Steps 6.1 through 6.3 until the final timestep.

The framework of the proposed DDU method is illustrated in Fig. 3. As an efficient framework, the multiscale finite volume method (MSFV) is usually used to describe flow processes due to its ability to simplify multi-scale interactions through operations like prolongation and restriction (Jenny et al., 2006; Künze et al., 2013; Lee et al., 2009; Lunati and Lee, 2009; Lunati et al., 2011; Zhou and Tchelepi, 2008). However, the direct application of MSFV to our approach is challenging due to the coupling of flow, heat transfer, and chemical reactions in ICP simulations. In this work, an edited Python programs is coupled with a widely applied thermal-reactive-compositional flow simulator, CMG-STARS (Hazra et al., 2013; Kelkar et al., 2011; Perez—Perez et al., 2019; Shen, 2009), to implement the DDU method. Alternatively, the simulator role of CMG-STARS can also be replaced by another appropriate opensource or commercial simulator.

# 4. Results and discussion

In this section, we conduct the thermal-reactive-compositional flow upscaling in homogeneous 3D ICP models with natural fractures. Firstly, the proposed DDU method is implemented on a dipped 3D model with five-point well pattern and natural fractures. Following that, the porosity and permeability of the dipped 3D model are changed to a series of different values to validate the reliability of the DDU method. Afterwards, to better represent the applicability of the DDU method on field-scale oil shale simulation, the DDU method is performed on a large 3D oil shale model with

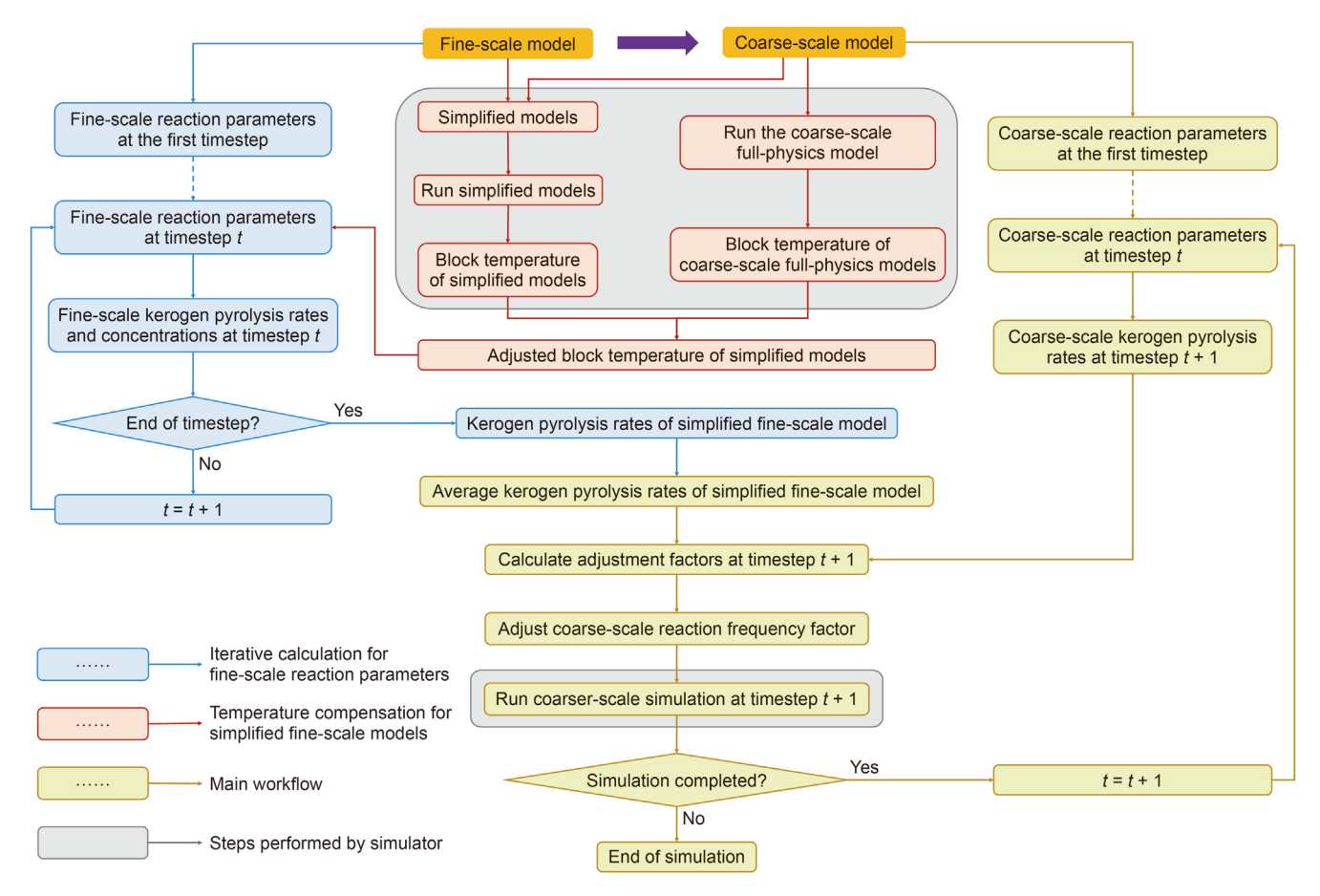


Fig. 3. The overall workflow of the DDU method.

fracture multiple hexagonal well patterns. At the end of this section, the enhancement in computational efficiency achieved by the DDU method is discussed. The pyrolysis reaction of the solid component (kerogen) dominates in those ICP simulations.

# 4.1. Case 1: Five-point well pattern in dipped oil shale reservoir with natural fractures

This work first applied the proposed DDU method to the scenario of a five-point well pattern in a dipped reservoir with natural fractures to test its performance. As shown in Fig. 4(a), a fine-scale 3D ICP model is constructed with  $25 \times 25 \times 25$  grid-blocks in x, y and z directions, respectively. The size of each block is  $0.5 \text{ m} \times 0.5 \text{ m} \times 0.1 \text{ m}$  in the x, y and z directions, individually. The model has two natural fractures that are modeled by EDFM and a 15° dip. The corresponding coarse-scale model is generated through the uniform coarsening of the fine-scale model. The coarse-scale model has  $5 \times 5 \times 3$  blocks with the block size of  $2.5 \text{ m} \times 2.5 \text{ m} \times 2.5 \text{ m}$  in the x, y and z dimensions, separately, as depicted in Fig. 4(b). Both the fine-scale and coarse-scale models contain a production well and four heater wells. The production well is located in the middle of the reservoir in the x-y plane, whereas the four heaters are situated at the four corners of the reservoir. The producer and four heaters perforate through all the vertical layers of the reservoir. The power for all the heaters is changing during the simulation, as presented in Fig. 5.

Adiabatic boundaries are used in all our models, and a kerogen pyrolysis reaction is specified, as shown in Table 1 (Burnham, 2015; Lee et al., 2016). Reservoir properties are provided in Table 2, and

the initial thermal conductivity for the rock, oil phase, gas phase, water phase and solid phase in all the models are listed in Table 3.

The DDU method is implemented on the coarse-scale model to obtain the upscaled model for Case 1. Figs. 6 and 7 demonstrate the kerogen pyrolysis rates for the well blocks and fracture blocks in Case 1. Considering the symmetry of the models, the kerogen pyrolysis rates of the blocks in the third layer are the same as that of the corresponding blocks in the first layer; therefore, Fig. 6 only presents the kerogen pyrolysis rates for one heater and the producer at the perforated blocks of the upper two layers. Similarly, Fig. 7 shows the kerogen pyrolysis rates for the four coarse-scale fracture blocks which include the reaction rate evolutions in the other fracture blocks.

It is witnessed in Fig. 6 that at the first-layer perforated block of the heater well, the coarse-scale kerogen pyrolysis rates display unreasonably larger peak values (0.55 kg/(m $^3$ ·day)) and end earlier (the 2170th day) than the fine-scale results, which top at 0.23 kg/(m $^3$ ·day) and end at the 2640th day. Conversely, the upscaled results greatly reduce the peak values to the same level as that of the fine-scale simulation, and the reaction duration is also closer to the fine-scale one. Besides, the fine-scale rates have multiple peak values due to the changes in heater power, which are not reflected in the coarse-scale results, whereas the upscaled results accurately capture the fine-scale variations. Thus, the upscaled results closely align with the fine-scale reaction rates.

Similarly, for the second-layer perforated block of the heater well, the coarse-scale peak value (0.64 kg/(m $^3$ ·day)) is twice as high as that of the fine-scale value (0.32 kg/(m $^3$ ·day)), and the coarse-scale reaction rates decrease to zero at the1930<sup>th</sup> day, which is

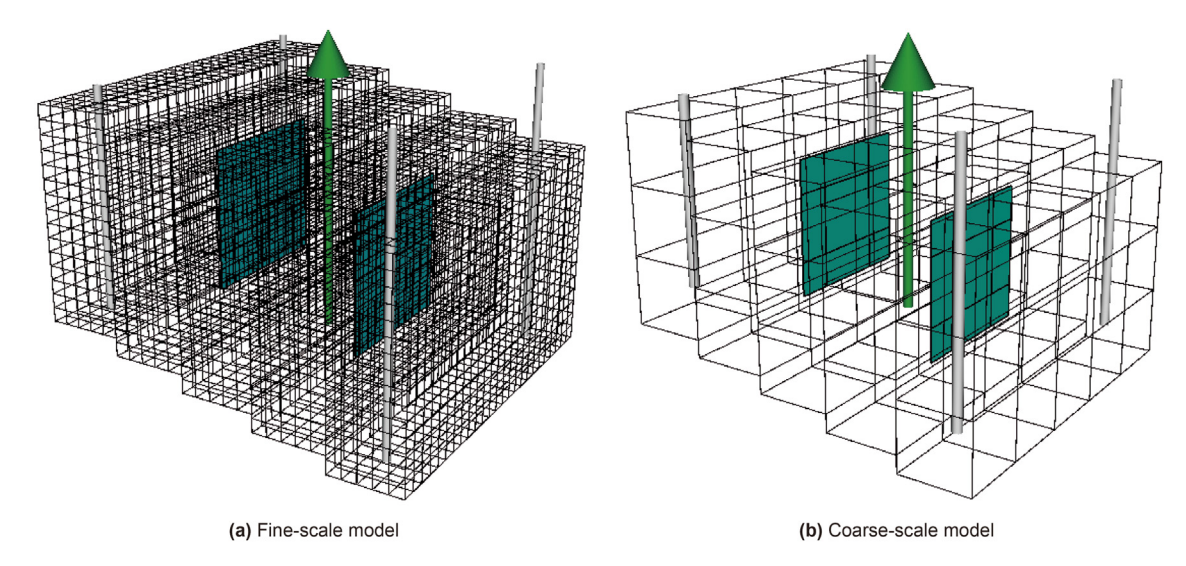


Fig. 4. ICP models in Case 1 (green cylinders: production wells; white cylinders: heater wells; light blue squares: natural fractures).

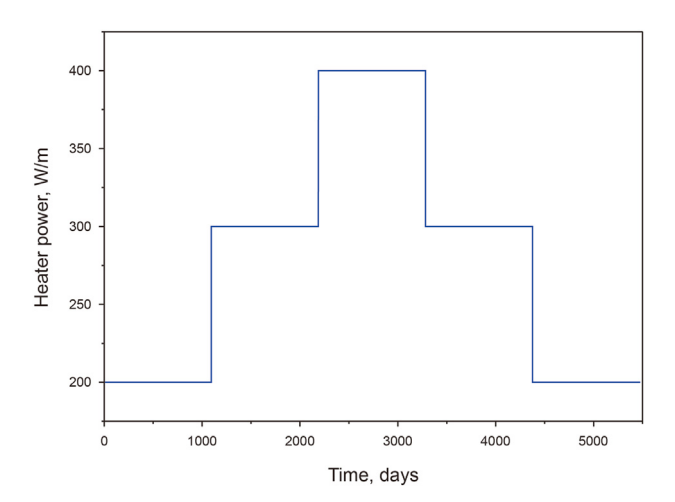


Fig. 5. Heater power evolution for the ICP model.

440 days earlier that the end of the fine-scale pyrolysis reaction at the 2370th day. In comparison, after the application of the DDU method, the difference between coarse-scale and fine-scale peak reaction rates is significantly reduced to 0.01 kg/(m $^3$ ·day), and the upscaled reaction time also fits better to the fine-scale one.

Concerning the first-layer perforated block of production well, Fig. 6 displays that the coarse-scale kerogen pyrolysis rates start at around the 3000th day, which is much later than the fine-scale one (the 2500th day). In addition, the kerogen in the coarse-scale block is still reacting actively at the end of the simulation, while the fine-scale kerogen is already depleted at the 4000th day. Apart from that, the coarse-scale peak reaction rate (0.16 kg/(m $^3$ ·day)) is less than half of the fine-scale peak value (0.38 kg/(m $^3$ ·day)). None-theless, after the implementation of the DDU method, the coarse-scale reaction rates start at the 2510th day and finish at the

**Table 2** Reservoir properties for the ICP models.

Reservoir properties	Values
Initial matrix porosity for fluid phase	0.0625
Initial matrix porosity for reactive solid phase	0.1875
Initial horizontal permeability of the matrix, mD	5
Initial vertical permeability of the matrix, mD	0.5
Initial fracture porosity for fluid phase	0.25
Initial fracture porosity for reactive solid phase	0.75
Initial fracture permeability, mD	10000
Initial reservoir temperature, °C	10
Bottom hole pressure, kPa	300

3770th day. Furthermore, the coarse-scale peak value is adjusted to 0.41 kg/( $\rm m^3$ ·day) in the upscaled results, which is much closer to the fine-scale results.

As for the reaction rates at the second-layer perforated block of the production well, it is depicted in Fig. 6 that the coarse-scale reaction time exhibits large discrepancies compared to the fine-scale results. The coarse-scale reaction rates rise from approximately the 3000th day, and reach the highest value of 0.19 kg/  $(m^3 \cdot day)$  at the 4170th day, followed by a steady decline to the 5000th day. In contrast, the fine-scale reaction rates soar at a much earlier date of the 2450th day, and hit the peak value of 0.52 kg/  $(m^3 \cdot day)$  at the 3100th day before dropping to zero at the 3450th day. Nevertheless, the upscaled reaction time matches closely with the fine-scale results, and the coarse-scale peak pyrolysis rate is also improved to 0.61 kg/( $m^3 \cdot day$ ) in the upscaled model. Therefore, the DDU method has considerably improved both the coarse-scale reaction time and peak value.

When it comes to the kerogen pyrolysis rates of the fracture blocks, Fig. 7 demonstrates that at the first fracture block, the coarse-scale reaction rates display inaccurate fluctuations and have much lower peak value (0.22 kg/(m $^3$ ·day)) compared to the fine-scale results. Moreover, the coarse-scale reaction time is largely

**Table 1**Chemical formula, reaction frequency factor, and activation energy of the kerogen pyrolysis reaction (Burnham, 2015; Lee et al., 2016).

Reaction	Chemical formula	Reaction frequency factor, s <sup>-1</sup>	Activation energy, J/mol
Kerogen pyrolysis reaction	Kerogen $\rightarrow$ 0.02691 H <sub>2</sub> O + 0.009815 C <sub>22</sub> H <sub>46</sub> + 0.01755 C <sub>11</sub> H <sub>24</sub> + 0.04002 C <sub>2</sub> H <sub>6</sub> + 0.01049 H <sub>2</sub> + 0.00541 CO <sub>2</sub> + 0.5828 prechar	$2\times10^{13}$	217664

**Table 3**The initial thermal conductivity of rock and fluid/reactive solid phase in I/(m·s·K).

Rock conductivity $\kappa_r$	Oil conductivity $\kappa_0$	Gas conductivity $\kappa_{\mathrm{g}}$	Water conductivity $\kappa_{\rm w}$	Solid conductivity $\kappa_s$
1.100	0.076	0.020	0.345	1.735

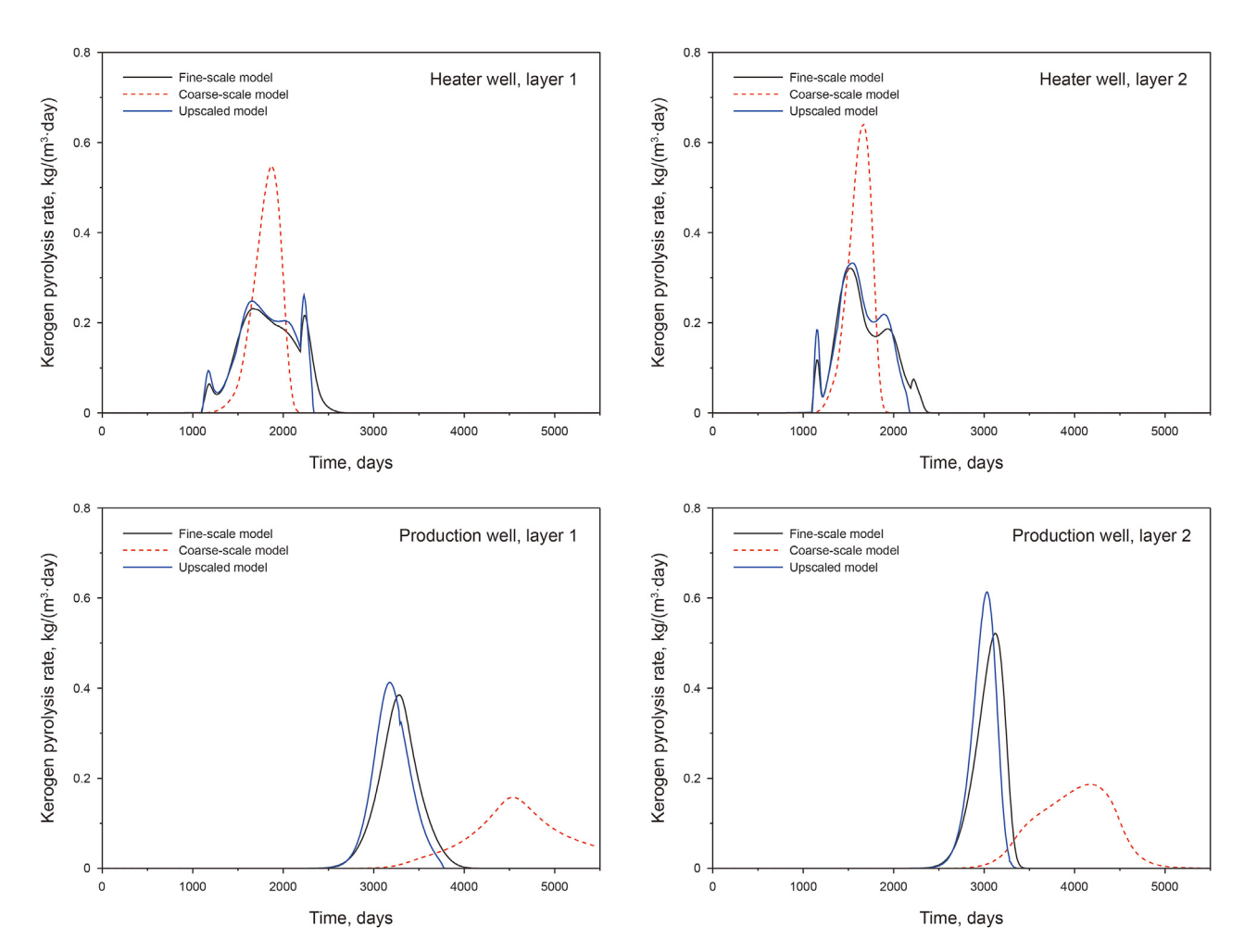


Fig. 6. Kerogen pyrolysis rates for the well blocks of the fine-scale, coarse-scale and upscaled models in Case 1.

deviated from the fine-scale reaction time. In contrast, the upscaled results corrected the deviations in reaction time, and greatly improved the peak of the coarse-scale kerogen pyrolysis rates to 0.61 kg/( $m^3$ ·day). Similar improvements in coarse-scale reaction rates can also be found in the results of the second and the fourth fracture blocks. It is noteworthy that for the third fracture block, the coarse-scale reaction rates are close to zero throughout the entire simulation, which is considerably different from the fine-scale results. On the contrary, the upscaled reaction rates match the fine-scale ones closely, which proves the effectiveness of the DDU method in capturing the fine-scale reaction dynamics.

For oil production, it is found in Fig. 8 that the coarse-scale oil rates fluctuate heavily from the 1840th day to the 2630th day. Apart from that, the peak value of coarse-scale oil rates (0.07  $\rm m^3/day)$  is lower than that of the fine-scale results (0.12  $\rm m^3/day)$ , leading to a much longer oil production period. In comparison, the upscaled oil rates almost coincide with the fine-scale ones. For instance, the highest value of the upscaled production rates is 0.13  $\rm m^3/day$ , and the start time and end time of the upscaled results also closely fit the fine-scale simulation. Similarly, Fig. 9 illustrates that the coarse-

scale cumulative oil production is constantly lower than that of the fine-scale results, whereas the upscaled curve almost overlaps the fine-scale one. Therefore, the DDU method effectively preserves the accuracy of the fine-scale simulations.

### 4.2. Effects of void porosity on the accuracy of the DDU method

The DDU method developed in this work utilizes the simplified models to approximate the fine-scale reaction rates. Considering the fact that the matrix void porosity (void porosity refers to the total porosity of fluid phase and reactive solid phase) and fracture void porosity of the simplified models are set to zero, the heat transfer caused by fluid phase and reactive solid phase is omitted in the simplified models, which gives rise to upscaling errors. Therefore, to further validate the accuracy of the DDU method, we have constructed a series of models with different matrix void porosity based on the fine-scale model in Case 1. The matrix void porosity of the fine-scale models built in this section varies from 0.05 to 0.45 with the step interval of 0.05, while the fracture void porosity of these models is a constant value of 1. The porosity of fluid phase is

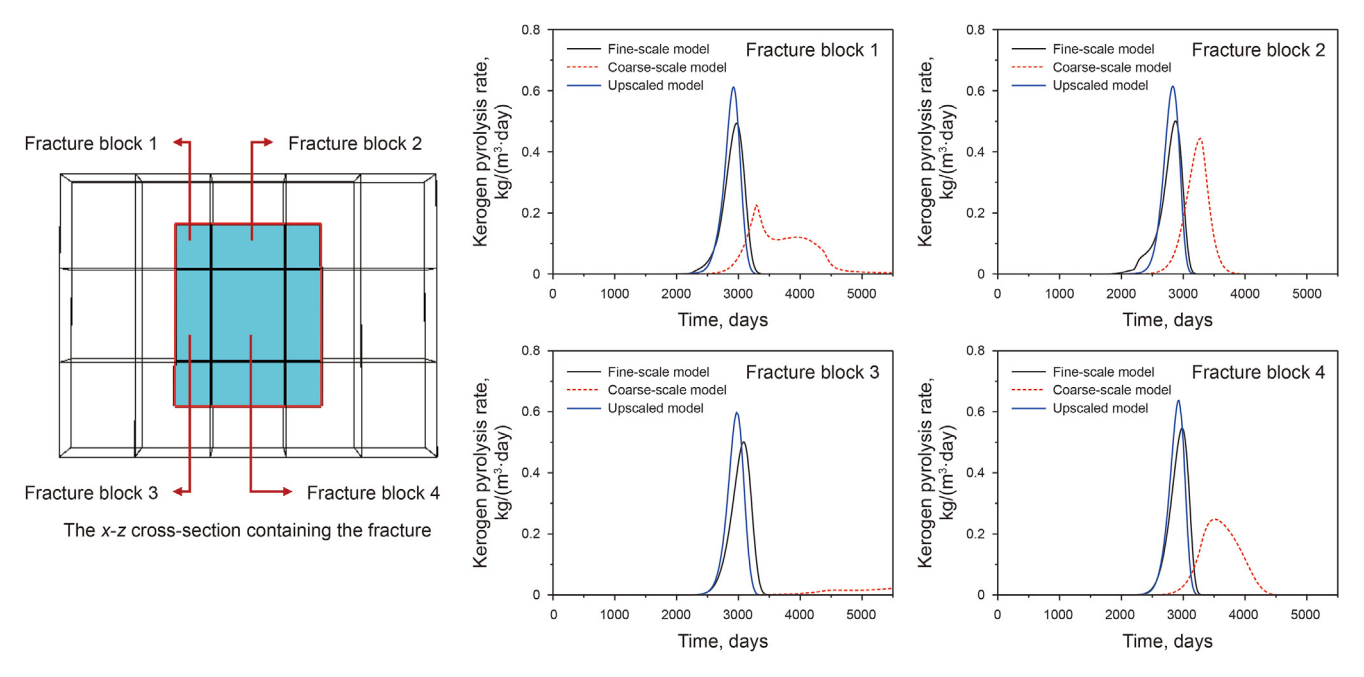


Fig. 7. Kerogen pyrolysis rates for the fracture blocks of the fine-scale, coarse-scale and upscaled models in Case 1.

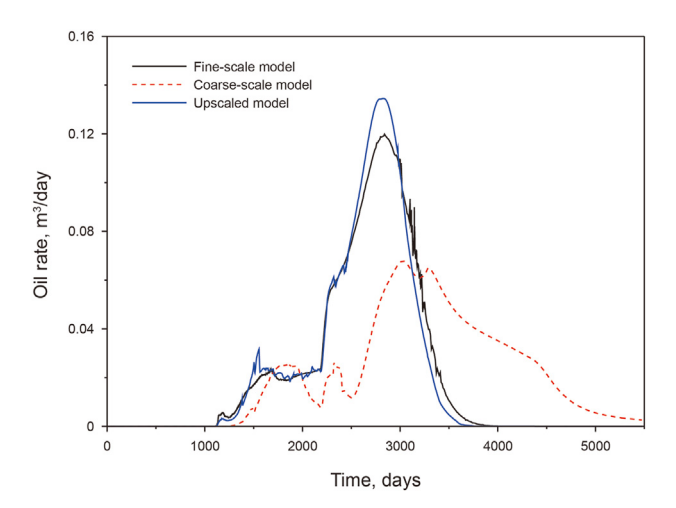


Fig. 8. Oil rates for the fine-scale, coarse-scale, and upscaled models in Case 1.

1/3 of the porosity of reactive solid phase. The other parameters of the models in this section are the same as that in Case 1.

Compared to the fine-scale model, the mean absolute error (MAE) were analyzed for the coarse-scale and upscaled oil production results. The MAE is given by

$$MAE = \frac{1}{n} \sum_{t=1}^{n} |Val_{f}^{t} - Val_{c/u}^{t}|,$$
 (20)

where n is the total timestep number;  $Val_{c/u}^t$  is the coarse-scale or upscaled parameter value at timestep t; and  $Val_{f}^t$  is the fine-scale parameter value at timestep t.

Further, a new parameter *IM* was introduced in this section to demonstrate the improvements in accuracy of the upscaled to the coarse-scale model by the DDU method, listed in Table 4. The improvements achieved by the DDU method (symbolized as "*IM*") is specified as

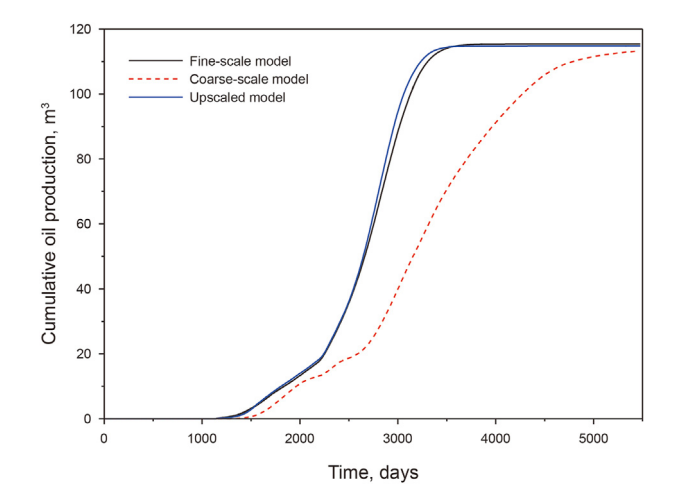


**Fig. 9.** Cumulative oil production for the fine-scale, coarse-scale, and upscaled models in Case 1.

$$\textit{IM} = \frac{MAE_c - MAE_u}{MAE_c} \times 100\%, \tag{21}$$

where  $MAE_c$  is the MAE of coarse-scale models; and  $MAE_u$  is the MAE of upscaled models. A closer  $\mathit{IM}$  to 100% implies that the upscaled results reduce more coarse-scale errors and match fine-scale results better. If  $\mathit{IM}$  equals 100%, it implies that the upscaling procedure eliminates all the coarse-scale errors and provides the same results as fine-scale simulation.

First and foremost, Fig. 10 demonstrates that both the coarse-scale and upscaled MAEs experience an upward trend as the matrix void porosity increases. As for the coarse-scale models, since the increments in void porosity enlarge fluid and reactive solid phase as well as their impacts on coarse-scale simulation results, and the coarse-scale model cannot accurately capture the dynamics of fluid and reactive solid phase, the MAE of coarse-scale models is in a positive correlation to the matrix void porosity. On the flip side,

 Table 4

 The MAE for the coarse-scale and upscaled models with different initial void porosity of the matrix, and the improvements achieved by the DDU method.

Parameter	Initial void porosity	MAE		IM, %
		Coarse-scale model	Upscaled model	
Cumulative oil production	0.05	2.496	0.126	94.95
	0.10	5.022	0.343	93.17
	0.15	7.634	0.545	92.86
	0.20	10.468	0.767	92.67
	0.25	14.000	0.897	93.59
	0.30	16.315	1.422	91.28
	0.35	19.638	1.515	92.29
	0.40	23.042	1.854	91.95
	0.45	26.620	2.090	92.15
Daily oil rate	0.05	0.004	$3.384 \times 10^{-4}$	91.54
	0.10	0.008	0.001	87.50
	0.15	0.011	0.001	90.91
	0.20	0.015	0.002	86.67
	0.25	0.019	0.003	84.21
	0.30	0.022	0.004	81.82
	0.35	0.025	0.005	80.00
	0.40	0.029	0.006	79.31
	0.45	0.032	0.007	78.13

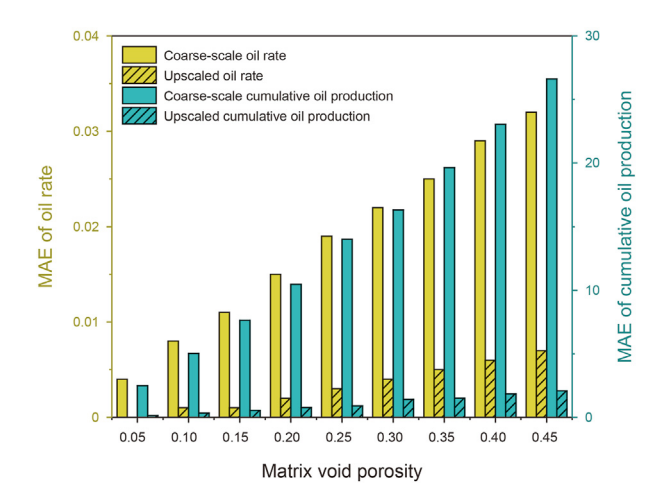
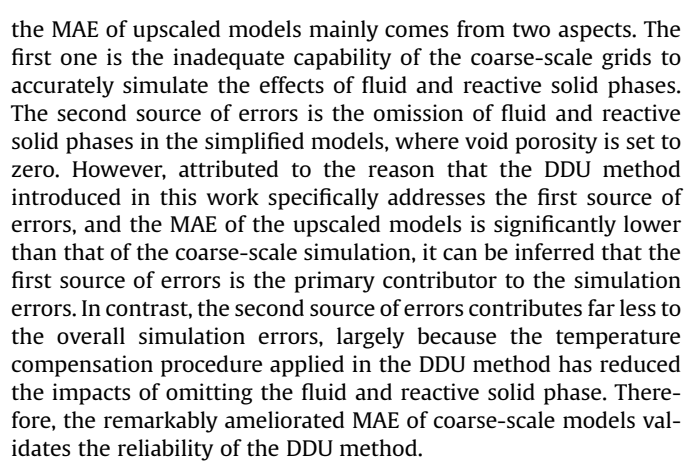


**Fig. 10.** The MAE of oil rates and cumulative oil production for the coarse-scale and upscaled models with different matrix void porosity.



As shown in Fig. 10, that the coarse-scale MAE for the oil rates grows rapidly from 0.004 at the void porosity of 0.05 to 0.032 at that of 0.045. However, the upscaled MAE is markedly lower than the coarse-scale MAE. A case in point is that at the void porosity of 0.05, the upscaled MAE is almost zero with the value of 3.384  $\times$  10 $^{-4}$ , which is ten times smaller than the corresponding MAE of the

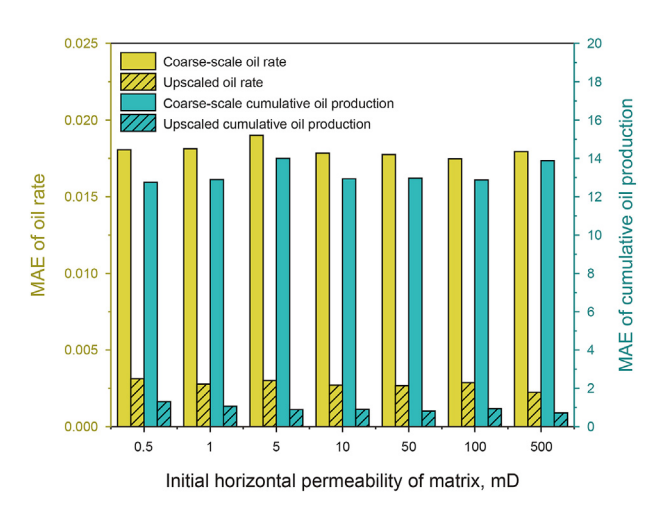


**Fig. 11.** The MAE of oil rates and cumulative oil production for the coarse-scale and upscaled models with different permeability values.

coarse-scale models. Furthermore, compared to the coarse-scale results, the MAE of the upscaled simulation only rises up to 0.007 when the void porosity reaches 0.45, indicating that the upscaled model has markedly reduced the coarse-scale simulation errors.

Similar phenomena are witnessed in the MAE of cumulative oil production. The MAE of coarse-scale models surged more than tenfold from 2.496 to 26.62 as the matrix void porosity goes up from 0.05 to 0.45. In comparison, the MAE of the upscaled results is 11.47—19.81 times less than the corresponding MAE of the coarse-scale results. Therefore, the DDU method can effectively preserve the high accuracy of fine-scale simulation in the dipped oil shale reservoir containing natural fractures and developed by changing heater power.

In terms of the improvements achieved by the DDU method (*IM*), it is observed in Table 4 that as the matrix void porosity rises, the *IM* for oil rates gradually decreases from 91.29% to 77.94% with small fluctuations, which suggests that larger matrix void porosity leads to lower *IM* for oil rates. On the contrary, the *IM* for cumulative oil production is consistently higher than 91.29% across the entire range of matrix void porosity. This denotes that the DDU method is more effective at enhancing the coarse-scale accuracy of cumulative oil production than oil rates.

 Table 5

 The MAE of coarse-scale and upscaled models with different initial absolute permeability of the matrix, and the improvements achieved by the DDU method.

Parameter	Initial absolute permeability, mD	MAE		IM, %
		Coarse-scale model	Upscaled model	
Cumulative oil production	0.5	12.743	1.306	89.75
•	1	12.898	1.073	91.68
	5	14.000	0.897	93.59
	10	12.935	0.905	93.01
	50	12.966	0.817	93.70
	100	12.878	0.944	92.67
	500	13.874	0.713	94.86
Daily oil rate	0.5	0.018	0.003	82.67
	1	0.018	0.003	84.71
	5	0.019	0.003	84.21
	10	0.018	0.003	84.79
	50	0.018	0.003	84.92
	100	0.017	0.003	83.55
	500	0.018	0.002	87.45

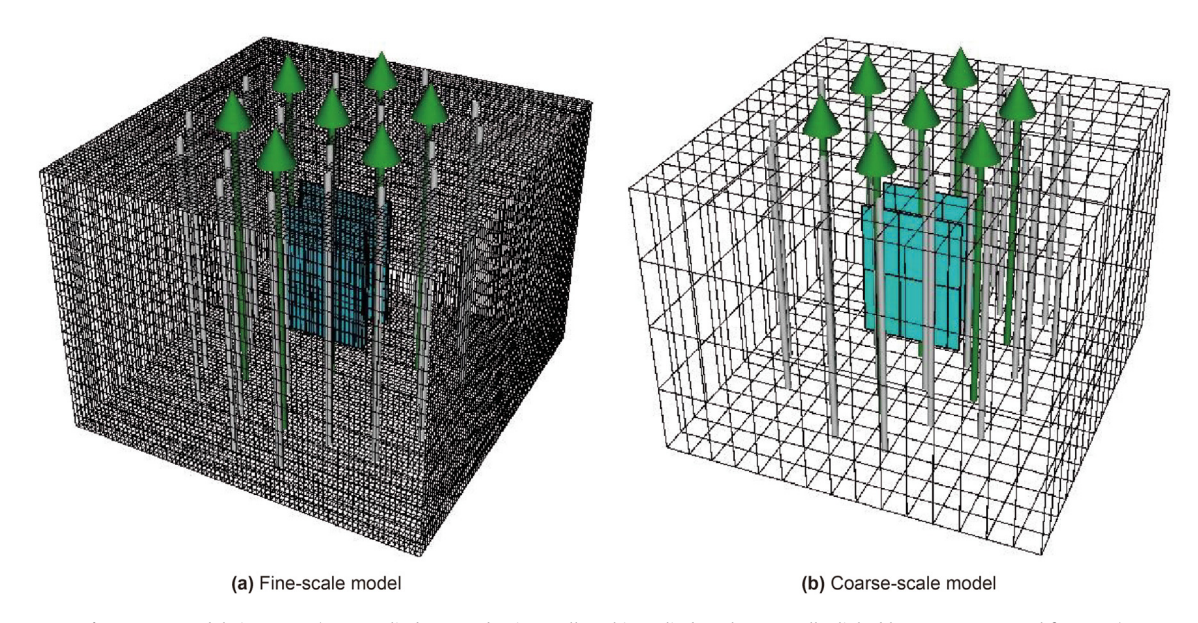


Fig. 12. ICP models in Case 2 (green cylinders: production wells; white cylinders: heater wells; light blue squares: natural fractures).

To sum up, the MAE for both coarse-scale and upscaled models goes upward as the matrix void porosity increases. On another aspect, although the simplified models omit the void porosity of matrix and fracture grid-blocks, the DDU method can still effectively and reliably reduce the coarse-scale errors throughout a large range of reservoir void porosity.

# 4.3. Effects of initial absolute permeability on the accuracy of the DDU method

In the simplified models, the omission of porosity also leads to the omission of permeability. Therefore, this section discusses the impacts of different initial absolute permeability on upscaling accuracy. Based on the fine-scale model in Case 1, we established a group of models with varying initial absolute permeability for matrix blocks. In those models, the initial horizontal permeability of matrix ranges from 0.5 to 500 mD, while the initial vertical permeability of matrix is 1/10 of the horizontal one. The initial absolute permeability of fracture grids is kept at a constant value of 10000 mD in all directions. The MAE of the oil rates and cumulative oil production for the models with different permeability values are depicted in Fig. 11, and the enhancements in accuracy achieved by the upscaling procedure are shown in Table 5.

It is witnessed in Fig. 11 that the MAE for the coarse-scale and upscaled models fluctuates slightly as the initial horizontal

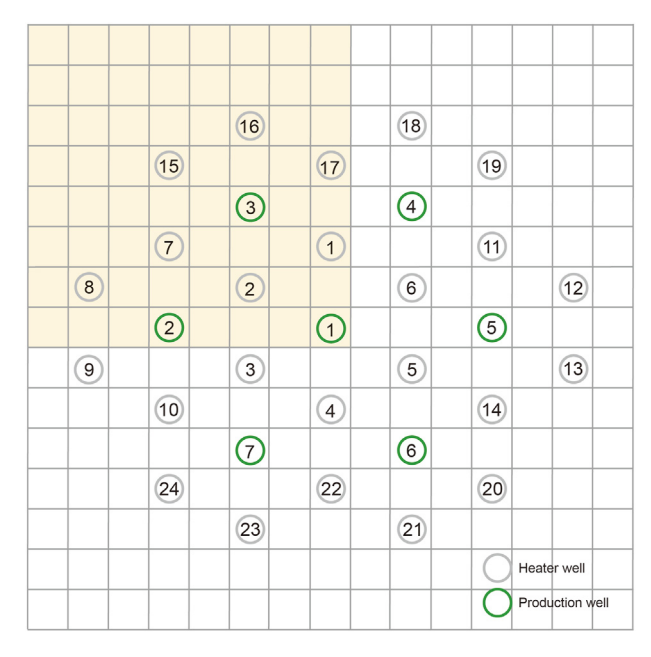


**Fig. 13.** The locations of production wells and heater wells for the coarse-scale model in Case 2.

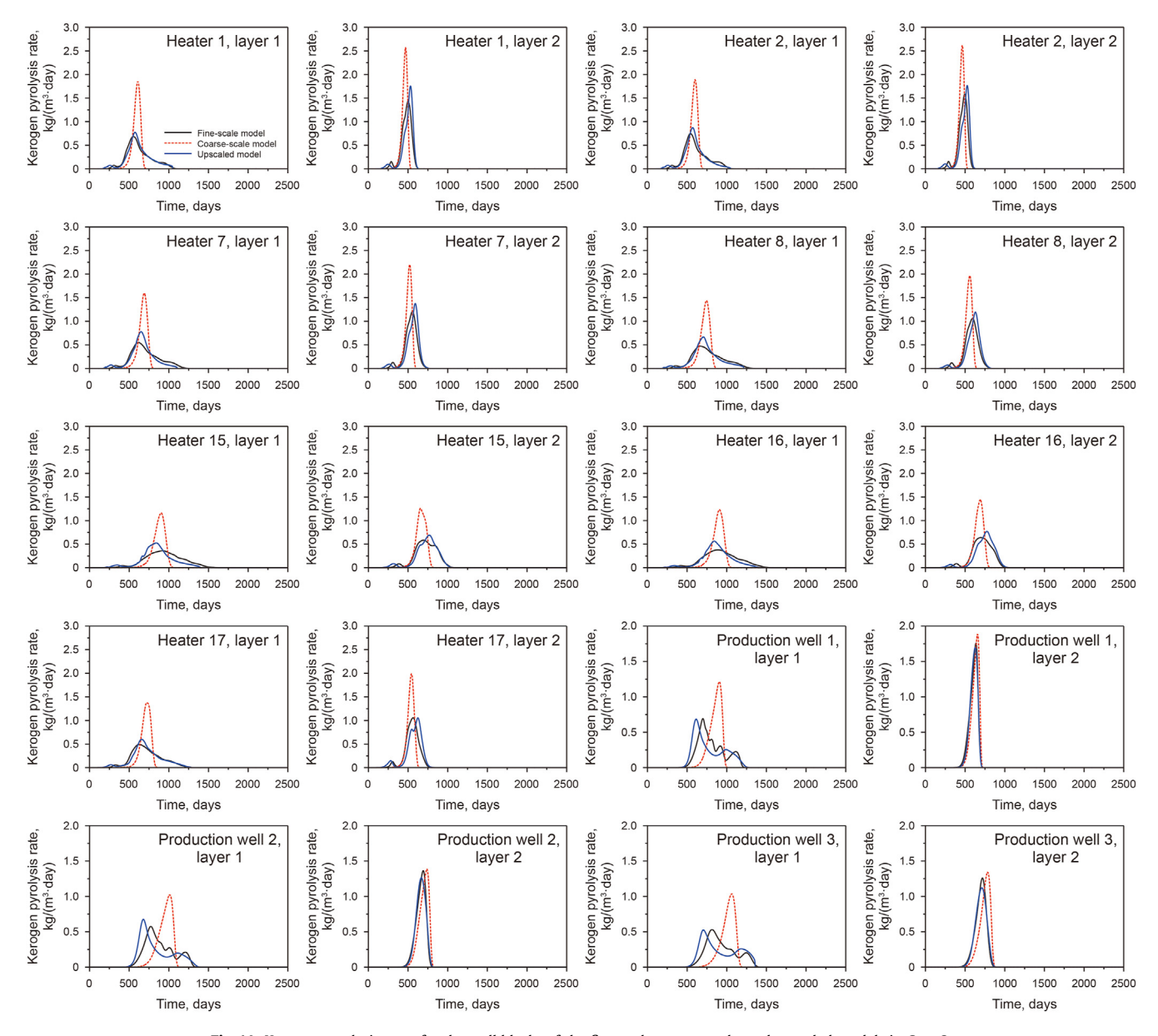


Fig. 14. Kerogen pyrolysis rates for the well blocks of the fine-scale, coarse-scale, and upscaled models in Case 2.

permeability increases from 0.5 to 500 mD. This denotes that the MAE of coarse-scale models is not sensitive to initial absolute permeability, which is attributed to the reason that as solid kerogen pyrolyzes, the enlarged fluid porosity increases the absolute matrix permeability according to Eq. (7), and thus the absolute permeability expands a large range during simulation. Similarly, the *IM* of the DDU method varies moderately within 4.78% for oil rates and 5.11% for cumulative oil production, and the changes are nonmonotonic as the initial horizontal permeability rises, suggesting that the initial absolute permeability does not significantly influence the performance of the DDU method.

However, the MAE of upscaled oil rates is 5.8—8.0 times smaller than that of the coarse-scale simulation, and the MAE of upscaled cumulative oil production is 9.8—19.5 times less than that of the coarse-scale results. The *IM* of the novel upscaled method is above 82.67% for oil rates and reaches 94.86% for cumulative oil production. These results indicate that the DDU method has drastically improved the coarse-scale accuracy.

4.4. Case 2: Large-scale hexagonal well patterns in naturally fractured oil shale reservoir

Based on the good performance of the proposed DDU method for a five-point well pattern in a dipped reservoir with natural fractures, this work further considers a larger oil shale reservoir with natural fractures and multiple hexagonal heater well patterns to verify its potential to be implemented in field-scale reservoir modeling. Firstly, a fine-scale ICP model is established with  $75 \times 75 \times 20$  grid-blocks in the x, y and z dimensions, respectively, as presented in Fig. 12(a). The size of each fine-scale block is  $0.5 \text{ m} \times 0.5 \text{ m} \times 2 \text{ m}$  in the x, y and z directions, respectively. Thus, the fine-scale model in Case 2 is 48 times the size of that in Case 1. The model contains two natural fractures and seven hexagonal well patterns comprising 7 production wells and 24 heater wells. The power for all the heaters is 400 W/m. The locations of production wells and heater wells are illustrated in Fig. 13. The corresponding coarse-scale model, which is built by the uniform coarsening of the

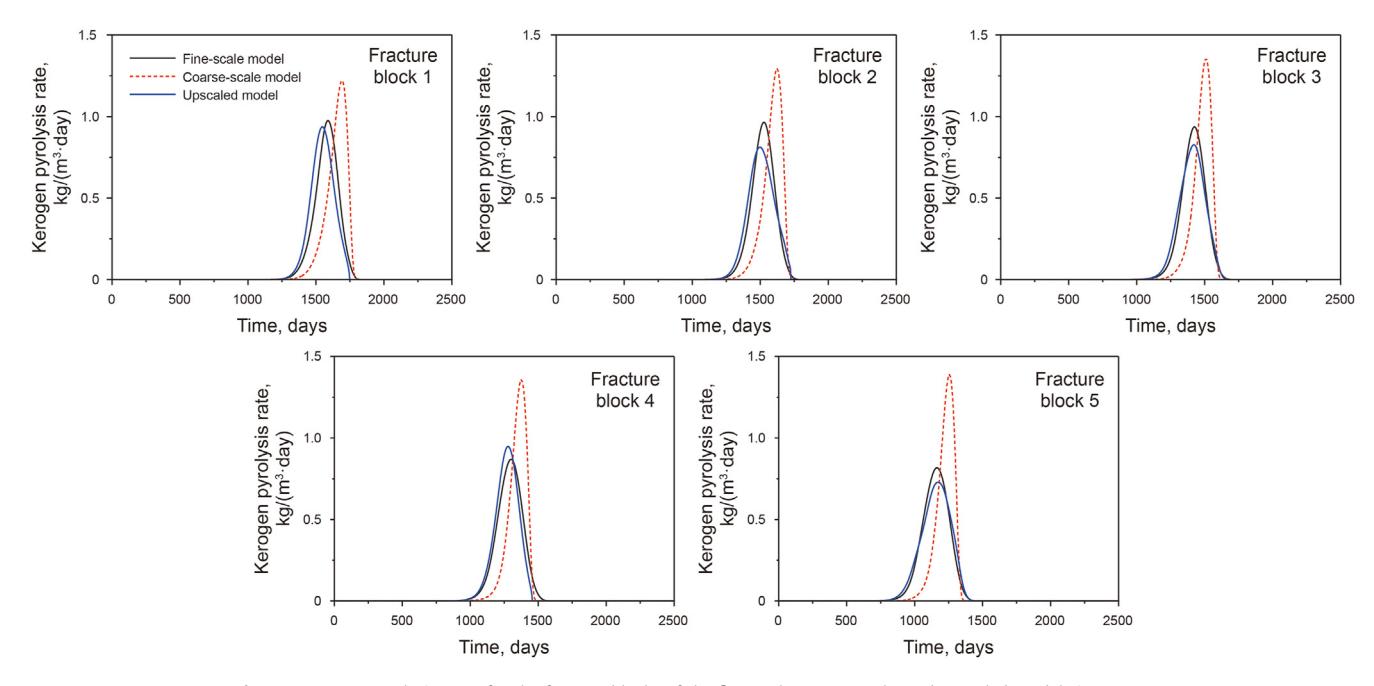


Fig. 15. Kerogen pyrolysis rates for the fracture blocks of the fine-scale, coarse-scale, and upscaled models in Case 2.

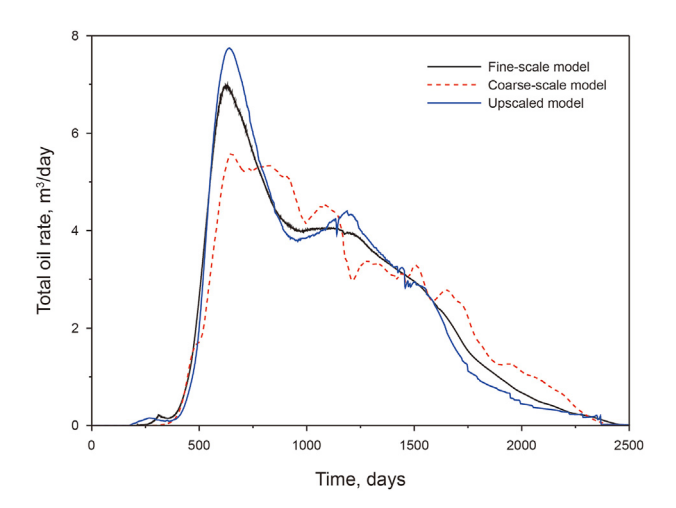
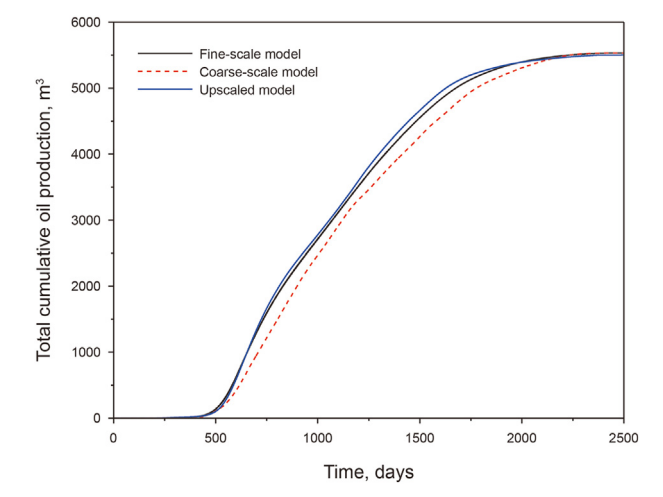


Fig. 16. Total oil rates for the fine-scale, coarse-scale, and upscaled models in Case 2.

fine-scale model, consists of  $15 \times 15 \times 4$  blocks with each block measuring  $2.5 \text{ m} \times 2.5 \text{ m} \times 10 \text{ m}$  in the x, y and z directions, separately, as shown in Fig. 12(b). The other parameters are the same as that in Case 1.

We implement the DDU method on the coarse-scale model to obtain the upscaled model for Case 2. Figs. 14 and 15 demonstrate the kerogen pyrolysis rates for the well blocks and fracture blocks. Due to the symmetry of the models, Fig. 14 only presents the kerogen pyrolysis rates for the grids containing the wells within the yellow region highlighted in Fig. 13, and the kerogen pyrolysis rates for the fracture grids shown in Fig. 15 also incorporate the evolution patterns of kerogen pyrolysis rates in other fracture blocks. For brevity, the legend is displayed only in the first sub-graph for both Figs. 14 and 15.

In terms of the first-layer perforated block of heater 1, Fig. 14 illustrates that the coarse-scale results experience unreasonably high peak value (1.832 kg/( $m^3$ ·day)) with reference to the fine-scale one (0.69 kg/( $m^3$ ·day)). Moreover, the coarse-scale reaction



**Fig. 17.** Total cumulative oil production for the fine-scale, coarse-scale, and upscaled models in Case 2.

**Table 6**Computational speedup achieved by the DDU method.

Case	Work type	Simulation runtime, min	Speedup
Case 1	Fine-scale simulation	8710	396
	Upscaling	22	
Case 2	Fine-scale simulation	241700	963
	Upscaling	251	

rates ended much earlier (the 728th day) than the fine-scale results (the 1051th day). After the implementation of the DDU method, the upscaled peak reaction rate is markedly ameliorated to 0.77 kg/ (m³·day), and the upscaled reaction time is closely aligned with the fine-scale simulation as well. More importantly, it is noteworthy that the fine-scale reaction rates demonstrate a short period of fluctuation from the 181th day to the 324th day for the first-layer perforated block of heater 1, and similar fluctuations can also be

found in the fine-scale results of other blocks perforated by heaters. Nevertheless, these phenomena are not shown in the curves of coarse-scale reaction rates. In contrast, the upscaled kerogen pyrolysis rates have accurately captured these variations, thus providing a precise match to the fine-scale results.

With respect to the fracture blocks, it is shown in Fig. 15 that the coarse-scale kerogen pyrolysis rates in the first fracture block rise later than the fine-scale rates, and illustrate a much larger peak value of 1.21 kg/(m³·day) at around the 1700th day. However, the fine-scale model tops at 0.98 kg/(m³·day) at the 1587th day. In comparison, the upscaled reaction rates reach the highest value of 0.93 kg/(m³·day) at the 1554th day, which fits closely to the fine-scale results. Similar improvements in reaction rates that are achieved by the DDU method can also be found in other well blocks and fracture blocks.

Fig. 16 illustrates the total oil rates for the ICP models in Case 2. The peak value of the coarse-scale oil rates is lower (5.55  $m^3/day$ ) compared to the fine-scale simulation (7.74 m<sup>3</sup>/day). The coarsescale oil rates exhibit marked fluctuations between approximately the 840th day and the 1650th day, leading to notable differences between the coarse-scale and fine-scale results. Conversely, the peak value of the upscaled model (6.96 m<sup>3</sup>/day) matches much closer to that of the fine-scale model, and the upscaled oil rates provide a smooth fit to the fine-scale ones. Fig. 17 displays that the total cumulative oil production of the coarse-scale model is consistently lower than the fine-scale results during the production period from the 500th day to the 2100th day, and the maximum difference between the coarse-scale and fine-scale cumulative oil production reaches 382.29 m<sup>3</sup>. However, it is noteworthy that the total cumulative oil production in the upscaled model almost coincides with the fine-scale simulation. Therefore, the DDU method has maintained the high accuracy of fine-scale simulation.

# 4.5. Simulation speedup of the DDU method

The enormous advantage of the upscaling method is to speed up the simulation, enhance the calculation efficiency and save time. To verify the speedup performance of the proposed DDU method, this section compared the overall simulation runtime for the fine-scale and upscaled models in Case 1 and Case 2, as listed in Table 6. All the simulations in this work are performed using six Intel Xeon Platinum 8260 CPU (2.4 GHz). The fine-scale simulation of Case 1 costs 8710 min (6 days approximately), while the upscaling method only consumes 22 min, which is remarkable improvement in computational efficiency with a speedup of 397 time. As for the large-scale models in Case 2, the fine-scale runtime reaches an astonishing 241700 min (about 168 days). In contrast, the upscaling procedure is completed within 251 min with a considerable computational speedup of 962 times. This suggests that the DDU method is highly efficient for large-scale solid-based thermalreactive-compositional flow simulations. Consequently, it can be implemented on the modeling of field-scale low-moderate maturity oil shale reservoirs to accurately forecast production performance, enhance optimization efficiency and accelerate decisionmaking processes.

#### 5. Conclusions

This work proposes a novel dual-model dual-grid upscaling (DDU) method for solid-based thermal-reactive-compositional flow modeling involving fracture grids. The DDU method utilizes simplified models to approximate the reaction kinetics of fine-scale simulations and equates the reaction rates of each coarse-scale grid block to the averaged fine-scale reaction rates within the corresponding coarse-scale block. This method is particularly suited for

fracture grids modeled independently of the surrounding rock volume and is compatible with both open-source and closed-source modeling software, as it does not require modifications to the underlying simulator source code. Based on the above discussion, the main conclusions of this study can be drawn as follows:

- (1) The DDU method integrates fracture and matrix upscaling while maintaining the accuracy of fine-scale simulations, and is applicable to 3D ICP simulations.
- (2) The proposed method provides significant computational savings, as demonstrated in 3D cases where the DDU method accelerates the fine-scale simulations by 396–963 times.
- (3) The proposed method has been successfully validated on large-scale oil shale models with hexagonal well patterns, proving its robustness and applicability for real-world reservoir modeling.

The results show that the DDU method effectively corrects coarse-scale errors in kerogen pyrolysis reaction rates, oil production rates, and cumulative oil production, achieving up to 94.95% accuracy improvement over coarse-scale models.

# **CRediT authorship contribution statement**

**Qi-Zhi Tan:** Writing — original draft, Methodology, Conceptualization. **Shu-Yang Liu:** Funding acquisition, Formal analysis. **Yan-Ji Wang:** Methodology. **Hang-Yu Li:** Validation, Data curation. **Jun-Rong Liu:** Investigation. **Wen-Yue Sun:** Visualization, Software.

#### **Declaration of interests**

The authors declare that they have no known competing financial interests or personal relationships that could have appeared to influence the work reported in this paper.

## Acknowledgments

The authors greatly acknowledge the financial support from the National Science Foundation of China (No. 52374063 and No. 52204065), the Natural Science Foundation of Shandong Province, China (No. ZR2023ME049 and No. ZR2021JQ18), and the Fundamental Research Funds for the Central Universities, China (24CX06017A).

#### References

Ahmed, Elfeel M., Geiger, S., 2012. Static and dynamic assessment of DFN permeability upscaling. In: SPE Europec/EAGE Annual Conference. https://doi.org/10.2118/154369-MS.

Alpak, F.O., Vink, J.C., 2016. Adaptive local-global multiscale simulation of the in-situ conversion process. SPE J 21 (6), 2112—2127. https://doi.org/10.2118/173218-PA. Aouizerate, G., Durlofsky, L.J., Samier, P., 2012. New models for heater wells in subsurface simulations, with application to the in situ upgrading of oil shale.

Comput. Geosci. 16 (2), 519–533. https://doi.org/10.1007/s10596-011-9263-1. Arrhenius, S., 1889. Quantitative relationship between the rate a reaction proceed and its temperature. J. Phys. Chem. 4, 226–248.

Barker, J.W., Thibeau, S., 1997. A critical review of the use of pseudorelative permeabilities for upscaling. SPE Reserv. Eng. 12 (2), 138–143. https://doi.org/ 10.2118/35491-PA

Bejan, A., 2013. Convection Heat Transfer. John Wiley & Sons. https://doi.org/ 10.1002/9781118671627.

Bogdanov, I., Mourzenko, V., Thovert, J.F., et al., 2003. Effective permeability of fractured porous media in steady state flow. Water Resour. Res. 39 (1). https://doi.org/10.1029/2001WR000756.

Burnham, A.K., 2015. A simple kinetic model of oil generation, vaporization, coking, and cracking. Energy Fuels 29 (11), 7156–7167. https://doi.org/10.1021/acs.energyfuels.5b02026.

Carman, P.C., 1997. Fluid flow through granular beds. Chem. Eng. Res. Des. 75, S32–S48. https://doi.org/10.1016/S0263-8762(97)80003-2.

Chen, T., Clauser, C., Marquart, G., et al., 2015. A new upscaling method for fractured

- porous media. Adv. Water Resour. 80, 60-68. https://doi.org/10.1016/ j.advwatres.2015.03.009.
- Durlofsky, L.J., 2005. Upscaling and gridding of fine scale geological models for flow simulation. In: 8th International Forum on Reservoir Simulation Iles Borromees. Stresa Italy
- Fan, Y., Durlofsky, L.J., Tchelepi, H.A., 2010. Numerical simulation of the in-situ upgrading of oil shale. SPE J. 15 (2), 368-381. https://doi.org/10.2118/118958-
- Farmer, C.L., 2002. Upscaling: a review. Int. J. Numer. Methods Fluid. 40 (1-2), 63-78. https://doi.org/10.1002/fld.267.
- Fowler, T.D., Vinegar, H.I., 2009, Oil shale ICP Colorado Field pilots, In: SPE Western Regional Meeting. https://doi.org/10.2118/121164-MS.
- Gong, B., Karimi-Fard, M., Durlofsky, L.J., 2006. An upscaling procedure for constructing generalized dual-porosity/dual-permeability models from discrete fracture characterizations. In: SPE Annual Technical Conference and Exhibition. https://doi.org/10.2118/102491-MS.
- Hazra, K.G., Lee, K.J., Economides, C.E., et al., 2013. Comparison of heating methods for in-situ oil shale extraction. In: IOR 2013-17th European Symposium on Improved Oil Recovery. https://doi.org/10.3997/2214-4609.20142631.
- Jenny, P., Lee, S.H., Tchelepi, H.A., 2006. Adaptive fully implicit multi-scale finitevolume method for multi-phase flow and transport in heterogeneous porous media. J. Comput. Phys. 217 (2), 627-641. https://doi.org/10.1016/ j.jcp.2006.01.028
- Kang, Z., Zhao, Y., Yang, D., 2020. Review of oil shale in-situ conversion technology.
- Appl. Energy 269, 115121. https://doi.org/10.1016/j.apenergy.2020.115121. Karimi-Fard, M., Gong, B., Durlofsky, L.J., 2006. Generation of coarse-scale continuum flow models from detailed fracture characterizations. Water Resour, Res. 42 (10). https://doi.org/10.1029/2006WR005015.
- Kelkar, S., Pawar, R., Hoda, N., 2011. Numerical simulation of coupled thermalhydrological-mechanical-chemical processes during in situ conversion and production of oil shale. In: 31st Oil Shale Symposium. https://api. semanticscholar.org/CorpusID:220042663.
- Koudina, N., Gonzalez Garcia, R., Thovert, J.F., et al., 1998. Permeability of threedimensional fracture networks. Phys. Rev. 57 (4), 4466-4479. https://doi.org/ 10.1103/PhysRevE.57.4466.
- Künze, R., Lunati, I., Lee, S.H., 2013. A multilevel multiscale finite-volume method. J. Comput. Phys. 255, 502–520. https://doi.org/10.1016/j.jcp.2013.08.042.
- Laidler, K.J., 1984. The development of the Arrhenius equation. J. Chem. Educ. 61 (6), 494. https://doi.org/10.1021/ed061p494.
- Lee, K., Moridis, G.J., Ehlig-Economides, C.A., 2016. A comprehensive simulation model of kerogen pyrolysis for the in-situ upgrading of oil shales. SPE J. 21 (5), 1612-1630. https://doi.org/10.2118/173299-PA
- Lee, S.H., Lough, M., Jensen, C., 2001. Hierarchical modeling of flow in naturally fractured formations with multiple length scales. Water Resour. Res. 37 (3), 443-455. https://doi.org/10.1029/2000WR900340.
- Lee, S.H., Zhou, H., Tchelepi, H.A., 2009. Adaptive multiscale finite-volume method for nonlinear multiphase transport in heterogeneous formations. J. Comput. Phys. 228 (24), 9036-9058. https://doi.org/10.1016/j.jcp.2009.09.009.
- Li, H., Vink, J.C., Alpak, F.O., 2015. An efficient multiscale method for the simulation of in-situ conversion processes. SPE J. 20 (3), 579-593. https://doi.org/10.2118/
- Li, H., Vink, J.C., Alpak, F.O., 2016. A dual-grid method for the upscaling of solidbased thermal reactive flow, with application to the in-situ conversion process. SPE J. 21 (6), 2097–2111. https://doi.org/10.2118/173248-PA.
- Li, L., Lee, S.H., 2008. Efficient field-scale simulation of black oil in a naturally fractured reservoir through discrete fracture networks and homogenized media. SPE Reservoir Eval. Eng. 11 (4), 750-758. https://doi.org/10.2118/103901-
- Liu, S., Gai, H., Cheng, P., 2023. Technical scheme and application prospects of oil shale in situ conversion: a review of current status. Energies 16 (11), 4386. https://doi.org/10.3390/en16114386.
- Long, J.C., Remer, J., Wilson, C., et al., 1982. Porous media equivalents for networks of

- discontinuous fractures. Water Resour. Res. 18 (3), 645-658. https://doi.org/ 10.1029/WR018i003p00645.
- Lunati, I., Lee, S.H., 2009. An operator formulation of the multiscale finite-volume method with correction function. Multiscale Model. Simul. 8 (1), 96-109. https://doi.org/10.1137/080742117.
- Lunati, I., Tyagi, M., Lee, S.H., 2011. An iterative multiscale finite volume algorithm converging to the exact solution. J. Comput. Phys. 230 (5), 1849–1864. https:// doi.org/10.1016/j.jcp.2010.11.036.
- Moinfar, A., Varavei, A., Sepehrnoori, K., et al., 2012, Development of a novel and computationally-efficient discrete-fracture model to study IOR processes in naturally fractured reservoirs. In: SPE Improved Oil Recovery Conference?. https://doi.org/10.2118/154246-MS.
- Moinfar, A., Varavei, A., Sepehrnoori, K., et al., 2013. Development of a coupled dual continuum and discrete fracture model for the simulation of unconventional reservoirs. In: SPE Reservoir Simulation Conference?, https://doi.org/10.2118/ 163647-MS.
- Nagy, T., Turanyi, T., 2011. Uncertainty of Arrhenius parameters. Int. J. Chem. Kinet. 43 (7), 359-378, https://doi.org/10.1002/kin.20551
- Oda, M., 1985. Permeability tensor for discontinuous rock masses. Geotechnique 35 (4), 483-495. https://doi.org/10.1680/geot.1985.35.4.483.
- Perez-Perez, A., Mujica, Chacín M., Bogdanov, I., et al., 2019. Simulations of in-situ upgrading process: interpretation of laboratory experiments and study of fieldscale test, SPE J. 24 (6), 2711–2730. https://doi.org/10.2118/190695-PA
- Shen, C., 2009. Reservoir simulation study of an in-situ conversion pilot of greenriver oil shale. In: SPE Rocky Mountain Petroleum Technology Conference. https://doi.org/10.2118/123142-MS
- Sherratt, J., Sharifi Haddad, A., Rafati, R., et al., 2020. A fracture upscaling method (FUM) for hydraulically fractured reservoirs; from discrete fracture modelling to finite difference simulations. J. Nat. Gas Sci. Eng. 83, 103611. https://doi.org/ 10.1016/j.jngse.2020.103611.
- Wellington, S.L., Berchenko, I.E., Rouffignac, E.P.D., et al., 2005. In situ thermal processing of an oil shale formation to produce a desired product. U.S. Patent No 6 880 633
- Xu, Y., Cavalcante Filho, J., Yu, W., et al., 2017. Discrete-fracture modeling of complex hydraulic-fracture geometries in reservoir simulators. SPE Reservoir Eval. Eng. 20 (2), 403-422. https://doi.org/10.2118/183647-PA.
- Xu, Y., Yu, W., Sepehrnoori, K., 2019. Modeling dynamic behaviors of complex fractures in conventional reservoir simulators. SPE Reservoir Eval. Eng. 22 (3), 1110-1130. https://doi.org/10.2118/194498-PA.
- Xu, Y., Lima, I.C.M., Marcondes, F., et al., 2020. Development of an embedded discrete fracture model for 2D and 3D unstructured grids using an elementbased finite volume method. J. Petrol. Sci. Eng. 195, 107725. https://doi.org/ 10.1016/j.petrol.2020.107725
- Yang, Z., Zou, C., Wu, S., et al., 2019. Formation, distribution and resource potential of the "sweet areas (sections)" of continental shale oil in China. Mar. Petrol. Geol. 102, 48-60. https://doi.org/10.1016/j.marpetgeo.2018.11.049.
- Yu, W., Gupta, A., Vaidya, R.N., et al., 2021. Efficient modeling of unconventional well performance with millions of natural and hydraulic fractures using embedded discrete fracture model EDFM. In: SPE Middle East Oil and Gas Show and Conference. https://doi.org/10.2118/204548-MS.
- Zhang, X., Ma, F., Yin, S., et al., 2021. Application of upscaling methods for fluid flow and mass transport in multi-scale heterogeneous media: a critical review. Appl. Energy 303, 117603. https://doi.org/10.1016/j.apenergy.2021.117603.
- Zhao, W., Hu, S., Hou, L., 2018. Connotation and strategic role of in-situ conversion processing of shale oil underground in the onshore China. Petrol. Explor. Dev. 45 (4), 563–572. https://doi.org/10.1016/S1876-3804(18)30063-6
- Zhao, W., Hu, S., Hou, L., et al., 2020. Types and resource potential of continental shale oil in China and its boundary with tight oil. Petrol. Explor. Dev. 47 (1), 1-11. https://doi.org/10.1016/S1876-3804(20)60001-5.
- Zhou, H., Tchelepi, H.A., 2008. Operator-based multiscale method for compressible flow. SPE J. 13 (2), 267-273. https://doi.org/10.2118/106254-PA.